Multivariable Adaptive Control of Thermal Properties During Welding

C. C. Doumanidis
Research Associate.

David E. Hardt
Associate Professor,

Laboratory for
Manufacturing and Productivity,
Massachusetts Institute of Technology,
Cambridge, MA 02139

Complete solution of the welding control problem involves regulating weld geometry, residual stresses, distortion and weldment metallurgical characteristics. The latter has been largely ignored in closed-loop control work, yet it is a basic determinant of weld integrity. In this paper, a previously developed input-output model for continuous regulation of the critical thermal properties of heat affected zone and cooling rate is used to develop a closed-loop MIMO control scheme. Since the physical system is non-linear and non-stationary, and process disturbances are reflected as model parameter changes, an adaptive control method is used. The implementation of the controller is based on deadbeat adaptive control, and it is applied to several different forms of the basic welding process model. The different models reflect a need to simplify the control system to accommodate available process measurements and hardware capabilities. A series of experiments performed on a robotic Gas Metal Arc welding system are presented that confirm the basic stability, robustness, adaptivity, tracking and disturbance rejection properties of the scheme. Bandwidth limitations are identified and improvements (primarily hardware oriented) are suggested.

Introduction

Improvement of fusion weld quality and productivity requires simultaneous regulation of several weldment characteristics. Although the relative importance of these welding outputs is application dependent, they can be categorized as follows:

(*a*) Weld bead location relative to the joint between parts.
(*b*) Weld bead cross section geometry.
(*c*) Thermally induced stress-strain effects, resulting in residual stresses and joint distortion.
(*d*) Metallurgical microstructure, the alterations of which during welding affects the final material properties.

The traditional method for obtaining the desired welding outputs depends on *a priori* conditioning of the welding inputs (such as heat input, travel speed and preheat conditions), usually on the basis of steady-state model input-output correlations. However, this static, empirical and open-loop approach has inherent disadvantages, including ambiguity during the welding transients (such as starting and stopping), sensitivity to process uncertainty (e.g., the usually unavailable arc efficiency, and weldment heat transfer characteristics), and sensitivity to unexpected process disturbances (such as part thickness variations). These shortcomings clearly suggest the alternative of employing feedback control of he important welding outputs, designed on the basis of available measurements and a suitable model of process and welding equipment dynamics.

The research described here concentrates on the development of such an in-process control system for welding outputs that describe the final metallurgical microstructure, and thus the material properties of the joint. Such properties have been largely ignored by control schemes in the welding literature, in spite of their importance to the process outcome.

While it is not practical to use feedback of metallurgical properties directly (because the necessary in-process sensing equipment is not well developed, and because of the large transportation lags involved), these can be measured and controlled indirectly. In fact, typical metallurgical transformations are well characterized by readily measurable weldment temperature field attributes, thus it is possible to employ closed loop control of such features while controlling the final microstructure and the resulting material properties in an open loop fashion (Doumanidis and Hardt, 1988). This is not overly restrictive, since most modeling uncertainities are related to, and most disturbances occur during, the welding process itself.

The control system design described here is developed by first defining several lumped outputs, derived from the distributed temperature field, that can adequately describe the microstructural changes during welding. These are then modulated using the heat source power and motion during welding. Although fusion welding is the focus of this investigation, the modeling and control methodology is directly applicable to analogous processes involving a moving heat source (arc cutting, LASER machining, etc.).

Welding Process Thermal Modeling

In previous work (Doumanidis and Hardt, 1988), it was suggested that the final microstructure and material properties

Contributed by the Dynamic Systems and Control Division for publication in the JOURNAL OF DYNAMIC SYSTEMS, MEASUREMENT, AND CONTROL. Manuscript received by the Dynamic Systems and Control Division July 1, 1988.
Associate Editor: G. E. Young.

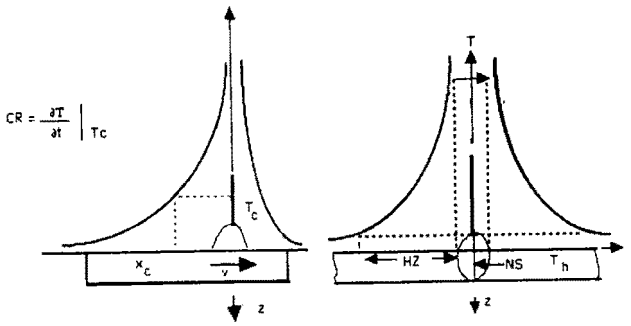

Fig. 1 Definition of the welding output NS, HZ, CR

of the joint can be adequately characterized by three lumped thermal welding outputs:

(*a*) The weld bead cross section NS, defined by the solidus isotherm T_m.
(*b*) The heat affected zone width HZ, measured between the weld bead and the enveloping isotherm T_h.
(*c*) The centerline cooling rate CR, defined at a critical temperature T_c which are illustrated in Fig. 1.

Analytic steady-state modeling of these temperature field characteristics based on pure conduction solutions (Rosenthal, 1941) demonstrated the sensitive and partially decoupled dependence of these outputs on three process variables, which are proposed as the welding inputs:

(*a*) The heat input Q_1 of the primary torch.
(*b*) The heat input Q_1 of the secondary torch, trailing at a fixed distance (required to separately modulate HZ and CR).
(*c*) The common velocity v of the two torches.

The nonlinear dynamic input-output relationships of this double torch configuration were modeled by an experimentally calibrated finite difference numerical simulation of the welding process (Doumanidis, 1986). The finite difference model itself was calibrated with a series of experiments using Gas Metal Arc (GMA) butt welding of thin mild steel plates (Doumanidis and Hardt, 1988). To facilitate the design of a control system, a locally linear dynamic model was established by fitting linear equations to both experimental data and finite difference simulations based on step inputs. Fixed parameter transfer functions were then derived from these equations.

For simple butt welding using GMAW, this linearized model, derived in the neighborhood of the nominal conditions:

$$Q_1^* = 2500 \qquad NS^* = 3.30 \text{ mm}^2$$
$$v^* = 5 \text{ mm/s corresponding to: } HZ^* = 5.39 \text{ mm}$$
$$Q_2^* = 0.0 \text{ W} \qquad CR^* = -82.2 \text{ K/s}$$

can be expressed in terms of the transfer functions:

$$\frac{NS}{Q_1}(s) = \frac{K_a}{(\tau_a s+1)} \qquad \frac{NS}{v}(s) = \frac{K_a'}{(\tau_a' s+1)} \qquad \frac{NS}{Q_2}(s) = 0$$

$$\frac{HZ}{Q_1}(s) = \frac{K_b\ (\tau_b s+1)}{(\tau_1 s+1)(\tau_2 s+1)} \qquad \frac{HZ}{v}(s) = \frac{K_b'\ (\tau_b' s+1)}{(\tau_1' s+1)(\tau_2' s+1)} \qquad \frac{HZ}{Q_2}(s) = \frac{K_b''}{(\tau_1'' s+1)} \tag{1}$$

$$\frac{CR}{Q_1}(s) = \frac{K_c}{(\tau_\alpha s+1)(\tau_\beta s+1)} \qquad \frac{CR}{v}(s) = \frac{K_c'}{(\tau_\alpha' s+1)(\tau_\beta' s+1)} \qquad \frac{CR}{Q_2}(s) = \frac{K_c''}{(\tau_\alpha'' s+1)}$$

where the parameter values identified are summarized in Table 1 for two different step input changes. Notice that the difference between the estimated values for positive and negative input steps indicates the nonlinearity of the original process,

Table 1 Gains and time constants of the linearized dynamic model

Input	Step	Output: Nugget Section NS (mm^2) K_a	T_a	Heat Affected Zone HZ (mm) K_b	T_b	T_1	T_2	Cooling Rate CR (K/s) K_c	T_α	T_β
q	+0.2 q^*	0.00574 mm^2/W	1.57 s	0.00356 mm/W	-1.56 s	5.42 s	0.50 s	0.0336 K/J	5.33 s	0.50 s
	-0.2 q^*	0.00434 mm^2/W	0.63 s	0.00221 mm/W	-1.78 s	2.75 s	0.33 s	0.0632 K/J	4.43 s	0.61 s
v	+0.2 v^*	-0.91 mm.s	1.78 s	-1.21 s	-1.39 s	3.04 s	0.52 s	-27.9 K/mm	4.61 s	0.45 s
	-0.2 v^*	-1.12 mm.s	4.95 s	-3.40 s	-1.16 s	11.0 s	0.65 s	-25.5 K/mm	6.02 s	0.41 s
q_2	+0.1 q^*	0 mm^2/W	0 s	0.00051 mm/W	0 s	2.65 s	0 s	0.0976 K/J	2.40 s	0 s
	-0.1 q^*	0 mm^2/W	0 s	0.00023 mm/W	0 s	2.41 s	0 s	0.1590 K/J	2.12 s	0 s

resulting in a nonstationary linearized model. Such nonlinear behavior is consistent with previously reported weld geometry dynamic models (Hardt et al., 1985; Suzuki and Hardt, 1987; Hale, 1989) and these others works also suggest (as will be shown below) that the process disturbances will also be reflected as model parameter changes.

Design of the Control System

The nonlinear, nonstationary nature of the processes model imposes several requirements on the control design. Among these are:

(*a*) Asymptotic stability of the closed-loop system in welding ranges of practical interest.
(*b*) Satisfactory time domain performance, i.e., zero steady-state error, limited settling time (with respect to the resulting weld length) and minimal overshoot in response to command inputs and disturbances.
(*c*) Robustness to the unmodeled dynamics of the welding process.
(*d*) Parameter adaptation to the structured uncertainty that arises from the nonlinearity of the process model, the initial error of experimentally measured parameters, their drift during welding, and abrupt changes in welding geometry, material properties, ambient conditions and process characteristics.
(*e*) Suitability of the control strategy to the input-output structure of the linearized process model. Moreover, since the process outputs are highly coupled, the control algorithm must be available in multivariable (MIMO), discrete-time form.

The proposed structure of the closed-loop control scheme is illustrated in Fig. 2. The output (temperature) measurements are used not only for the evaluation of the welding outputs NS, HZ, CR, but also for he identification of the dynamic

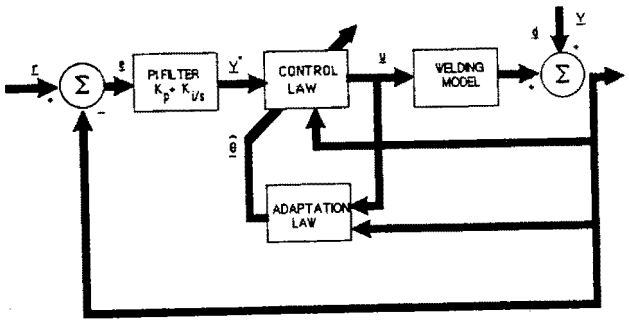

Fig. 2 The double-loop structure of the control system

model parameters, required for the in-process tuning of the controller.

Because of these requirements, a discrete-time, multivariable, adaptive deadbeat control algorithm from Goodwin et al. (1980), was chosen, and its MIMO, indirect, orthogonal projection version is adopted here. This is based on a discrete time matrix fraction or autoregressive moving average (ARMA) form of the sampled system (for sampling period T). This was obtained from the continuous-time linearized model (equation (1)) by replacing the elemental transfer functions by their zero-order-hold (ZOH) equivalent pulse transfer functions (Astrom 1985), and writing them as a set of concatenated MISO systems with a common input vector:

$$[\mathrm{diag}(A_i(q^{-1}))]\, y(t) = [q^{-d_{ij}} B_{ij}(q^{-1})]\mathbf{u}(t) \tag{2}$$

$$[y_i(t+d_i)] = [\mathrm{diag}(\alpha_i(q^{-1}))]\mathbf{y}(t) + [\beta_{ij}(q^{-1})]\mathbf{u}(t) \tag{3}$$

where $i = 1 \ldots m$ with m = number of outputs = 3

and $j = 1 \ldots r$ with r = number of inputs = 3.

The last equation is obtained by recursive substitutions. In these expressions, $\mathbf{u}(t) = [Q_1\ v\ Q_2]^T$ and $\mathbf{y}(t) = [\mathrm{NS\ HZ\ CR}]^T$ are the welding input and output vectors and:

$$A_i(q^{-1}),\ B_{ij}(q^{-1})$$

$$\alpha_i(q^{-1}) = \sum_{k=0}^{n_i-1} a_i{}^k q^{-k}, \quad \beta_{ij}(q^{-1}) = \sum_{i=0}^{m_i+d_i-1} b^1{}_{ij} q^{-1}$$

are scalar polynomials in the unit delay operator q^{-1}, with:

$$d_i = \min_j \{d_{ij}\}, \text{ (the system delays)}$$

$$n_i = \deg(A_i(q^{-1})), \text{ and}$$

$$m_i = \max\{\deg(q^{d_i - d_{ij}} B_{ij}(q^{-1}))\}.$$

The following assumptions are made about the samples system:

1. The system delays d_i are known exactly. Further, it is assumed that the sampling period T is long enough to cover the process delays, plus the thermal measurement, algorithm computation and actuator reaction times, so that the welding inputs affect the welding outputs of the next sampling instant. Thus $d_i = 1$.

2. The polynomial orders n_i and m_i are known to an upper bound, i.e., $n_1 = 2$, $n_2 = 5$, $n_3 = 5$, $m_1 = 1$, $m_2 = 4$, $m_3 = 4$, as suggested by the discretized linear model.

3. The sampled process has a stable inverse, i.e., no zeros output side the unit disk of the z-plane:

$$\det[z^{(d_{ij}-d_i)} B_{ij}(z)] \neq \text{ for } |z| \leq 1.$$

Since the continuous-time process displays nonminimum-phase behavior and delays (see equation (1)), and thus does not have a stable inverse, a long enough sampling period T is needed to move the unstable zeros of the pulse transverse functions inside the unit disk (Astrom and Wittenmark, 1984) so the sampled process can satisfy the inverse stability condition (or solvability or linear boundedness of the inputs by the outputs).

Under these assumptions the following parametrization is defined:

Parameter vectors:

$$\Theta_i{}^o = [(a_i{}^k,\ k = 0..n_i - 1),\ ((b_{ij}{}^1,\ j = 1..r),\ 1 = 0..m_i + d_i - 1)]^T \tag{4}$$

Augmented vectors:

$$\Phi_i(t) = [(y_i(k),\ k = t..t - n_i + 1),\ (\mathbf{u}^T(1),\ 1 = t..t - m_i - d_i + 1)]^T \tag{5}$$

where both $\Theta_i{}^o$ and $\Phi_i(t)$ vectors are of order $n_i + r\,(m_i + d_i)$. In these terms the ARMA model is written as:

$$y_i(t + d_i) = \Phi_i{}^T(t)\ \Theta_i{}^o \tag{6}$$

and the desired (model) output $\mathbf{y}^*$ can be tracked as follows:

$$y_i{}^*(t + d_i) = \Phi_i{}^T(t)\ \Theta_i(t). \tag{7}$$

This last expression, which forms the basis of the deadbeat control law, represents a set of m equations solvable for the r unknown components of $\mathbf{u}(t)$ after some delay. Since the vectors Θi^o of the actual parameters are not known, they must be estimated in-process by the adaptation law:

$$\hat{\Theta}_i(t) = \hat{\Theta}_i(t-1) + \gamma(t)\ \Phi_i\ (t - d_i)\ [1 + \Phi_i{}^T\ (t - d_i)\ \Phi_i(t - d_i)]^{-1}\ [y_i(t) - \Phi_i{}^T(t - d_i)\ \hat{\Theta}_i(t-1)] \tag{8}$$

where (t) is the adaptation gain. Thus the parameter error is given by a scaled orthogonal projection of the augmented vector $\Phi_i(t - d_i)$ on the hypersurface of an estimate of the output error.

Under these conditions, it is shown in Goodwin et al. (1980) that the input $\mathbf{u}(t)$ and output $\mathbf{y}(t)$ remain bounded at all times, and the output tracking objective is asymptotically satisfied:

$$y_i(t) - > y_i{}^*(t) \text{ as } t - > \infty$$

Also, the Euclidian norm of the parameter deviations $\hat{\Theta}_i(t) = \Theta_i(t) - \Theta_i{}^o$ converges asymptotically, although not necessarily to zero:

$$\|\hat{\Theta}_i(t)\|^2 - \|\hat{\Theta}_i(t-1)\|^2 < 0 \text{ for } t > 0.$$

Moreover, it is indicated that this linear, time-invariant (LTI) analysis is applicable to processes with cone-bounded nonlinearities and slow enough time variation of the parameters $_i{}^o$ relative to the sampling period T. Finally, robustness against unmodeled dynamics can be ensured by sampling slowly enough, albeit at the sacrifice of bandwidth (Valavani, 1986; Rohrs and Sirriani, 1986).

Some additional modifications are combined with the original algorithm. Thus, welding input saturation with anti-reset windup (Astrom and Wittenmark, 1984) is added to the controller, to avoid excessive penetration (burn-though), lack of fusion and excessive porosity. Also, in order to ensure the inverse stability (assumption 3) in real time, the adaptation gain $\gamma(t)$ is varied so as to avoid singularities of the control law and to optimize the conditioning of the matrix of leading parameters, i.e., det $[b_{ij}{}^o]$. Moreover, an external secondary loop is employed, as in the double-loop configuration of Fig. 2, with low-pass PI filters in its feedforward path, in order to attenuate the high-frequency components of the typical deadbeat responses of the internal primary loop, and to provide additional design flexibility in adjusting the transient response.

Based on the linear system model (equation (1)), a *standard* 3×3 controller is designed according to the above algorithm, and this design comprises 46 components of the parameter vector $\hat{\Theta}_i$, and a sampling period T = 2s to compensate for the non-minimum phase dynamics and process delays. Because of the large order of $\hat{\Theta}_i$, a *simplified* 3×3 controller is similarly developed. In this case the HAZ width is controlled indirectly through the total T_h-isotherm width w_h (which avoids the non-minimum phase dynamics of HZ introduced by the T_m - isotherm, Doumanidis and Hardt, 1988). Also, the HZ/$Q_2(s)$

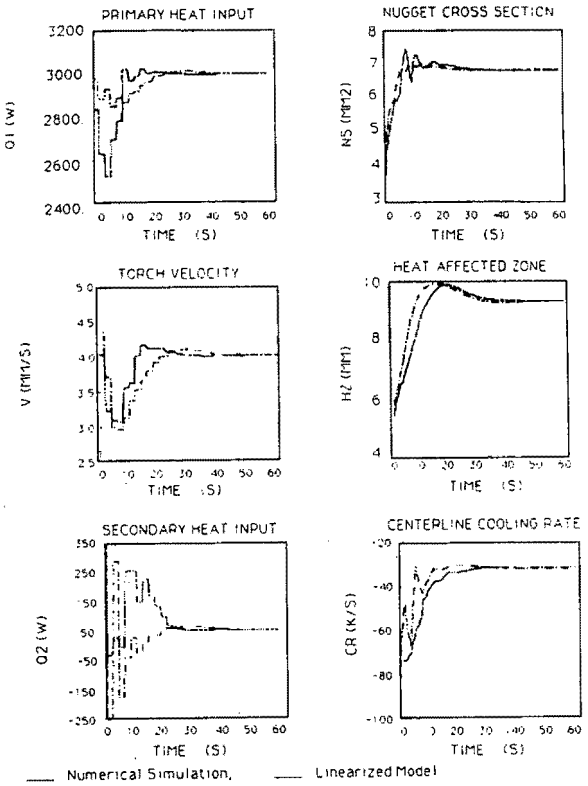

Fig. 3 Time responses of the welding outputs and inputs after a step reference command (*standard 3×3 controller*)

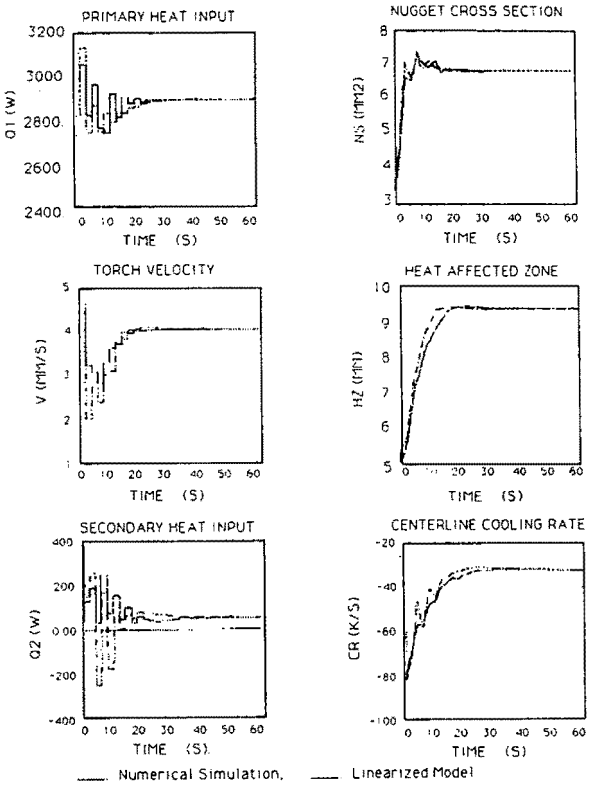

Fig. 4 Time responses of the welding outputs and inputs after a step reference comand (*simplified 3×3*) controller

coupling as well as the secondary modes of $CR/Q_1(s)$ and $CR/v(s)$ were ignored in the controller parametrization.

These design simplifications enable the reduction of the controller parameters in Θ_i to 24 and the sampling period to T = 1s, and improve the conditioning of the control law. In both controllers, an initial estimate of the leading parameters in $\hat{\Theta}_i(0)$ is obtained by discretization of he continuous-time linear process model, with parameter values selected in the ranges of Table 1, so as to match the open-loop responses of the calibrated numerical simulation to the tests of the next section.

Closed-Loop Performance

Using these two controller designs, the performance of the closed-loop control system was assessed by simulation. Both the linearized model and the numerical simulation were used as the process model, and all such simulations were based on butt welding of 3.17mm (1/8 in.) thick mild steel start at the nominal conditions stated above. Thus, the transient response during an in-process change of the operating point was tested during a substantial step reference command at $t=0$ to the desired welding outputs:

$$NS_d = 6.83 \text{ mm}^2 \qquad Q_1 = 3000 \text{ W}$$

$$HZ_d = 9.21\text{mm} \quad \text{corresponding to:} \quad v = 4\text{mm/s}$$

$$CR_d = -32.2\text{K/s} \qquad Q_2 = 50.0\text{W}$$

The closed-loop responses of the welding outputs and inputs are shown in Fig. 3 for the *standard 3×3* controller and in Fig. 4 for the *simplified 3×3* controller. The dot-dashed line was obtained using the linearized dynamic model, and the solid line with the full numerical simulation as the process model.

The regulator performance in maintaining the specified nominal conditions in the presence of unexpected disturbances, was tested during a step change of the plate thickness at $t=0$, from 3.17 to 2 mm. While such disturbances can be directly handled by the numerical process model, they were modeled as equivalent additive output disturbances for the linearized process model (see Fig. 2), characterized by the numerical simulation open-loop response as:

$$\text{NS: } d_{NS}(t) = 2.46\,[1-\exp(-t/1.36)] \text{ (mm}^2\text{)}$$

$$\text{HZ: } d_{HZ}(t) = 4.34\,[1-\exp(-t/6.43)] \text{ (mm)}$$

$$\text{CR: } d_{CR}(t) = 32.48\,[1-\exp(-t/3.12)] \text{ (K/s)}$$

The closed-loop welding output and input responses to this disturbance are given in Figs. 5 and 6 for the *standard 3×3* and *simplified 3×3* controllers, respectively, using both the linearized model (dot-dashed line) and the numerical simulation (solid line) as the process model. As before, the difference between these two model response is because of parameter errors, unmodeled dynamics and errors in the linear approximation of the process.

These servosystem and regulator performance tests demonstrate the asymptotically stable reference command following and disturbance rejection performance of the control system, and in spite of the nonsmooth transients caused by the abrupt input modulation by the dead-beat controller and the dramatic variations, there is no error at the steady state. In both tests the parameter vectors of the indirect adaptive controller Θ_i eventually converge close to their expected values Θ_i^o, indicating good handling of the structured uncertainty. The robustness to unstructured uncertainty is evident from the similarity of the closed-loop responses obtained using two process models with different dynamics (linearized model, numerical simulation), and two controllers with different parametrizations (*standard 3×3*, *simplified 3×3*). As regards the closed-loop bandwith, the difference between the responses obtained with the *standard 3×3* controller, (which show no substantial improvement over the open-loop bandwith), and those obtained with the *simplified 3×3* controller, is because

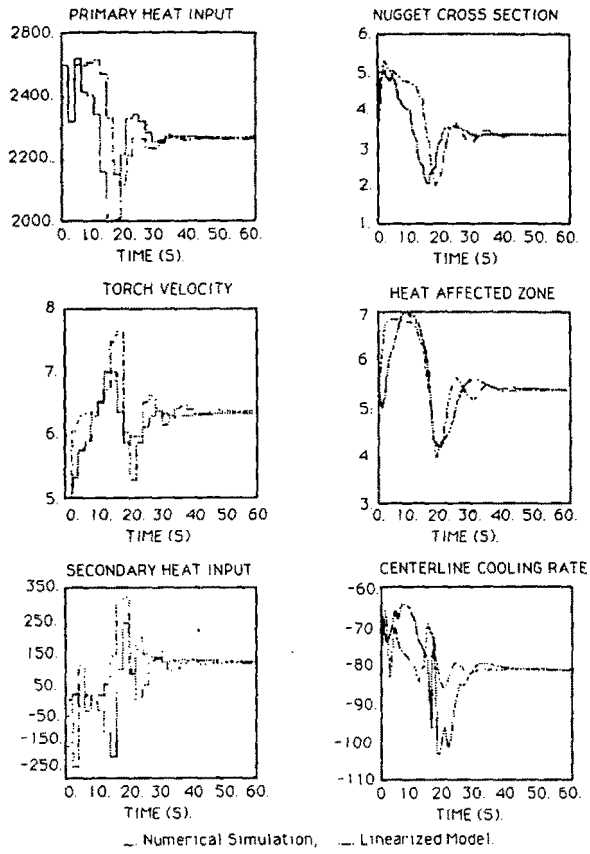

Fig. 5 Time responses of the welding outputs and inputs after a step disturbance (*standard* 3×3 controller)

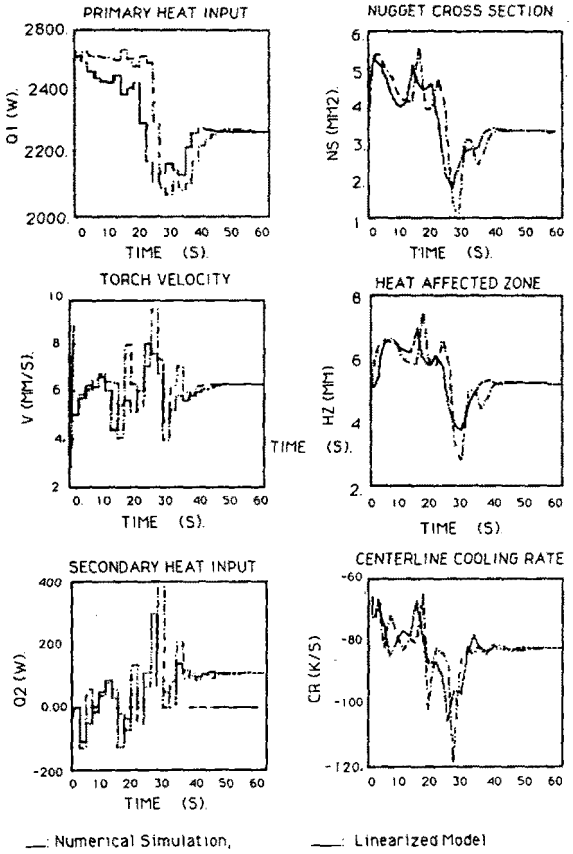

Fig. 6 Time responses of the welding outputs and inputs after a step disturbance (*simplified* 3×3 controller)

of the shorter sampling period and more efficient parametrization of the latter, which promote the better controller conditioning, adaptation on a finer time scale and faster parameter convergence. However, as discusssed in Doumanidis 1988), a decrease in the sampling period T is at the expense of the closed-loop stability (assumption 3) and robustness (Rohrs ad Sirriani, 1986), and ultimately limited by the speed of the actual sensor, actuator and controller.

The 2×2 Process Model

As suggested in Fig. 7, a considerable number (≥ 12) of spot temperature measurements on the top and bottom plate surfaces is required for the real-time evaluation of the welding outputs, necessitating a complicated sensor setup, a long sequential measurement time (0.5s per point with the 2-D infrared camera system used for the subsequent experiments (Inframetrics, 1985), and extensive computational requirements for the isotherm interpolation among distinct point temperatures. Also, the separate double torch configuration introduces the cost and complexity of two independently controlled power supplies, as well as electromagnetic interaction between the arcs. Finally, the extensive controller parametrization of both the *standard and simplified* controllers for the 3×3 process model is rather demanding in terms of real-time computational requirements. All these equipment limitations suggest a reduction of the process model and redefinition of the welding inputs and outputs, so as to ensure a short sampling period, frugal parametrization, and thus the desired closed-loop performance.

Considering the welding ouputs in Fig. 7, the weld bead cross section NS is the most problematic from the control viewpoint, because it cannot be directly measured. While Fig. 7 shows the use of bottomside temperatures to estimate NS, even such cumbersome measurements do not insure accurate

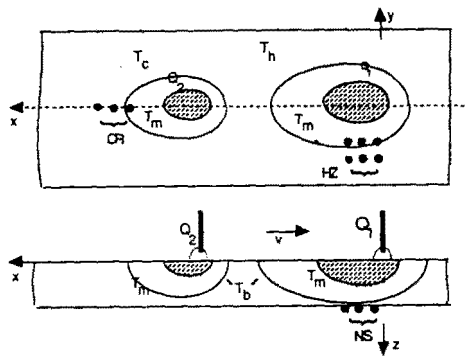

Fig. 7 The temperature measurements system

estimation of NS as demonstrated by Nomura (1978). Thus, NS was temporarily abandoned as a welding output, in anticipation of its indirect control by a separate weld bead geometry controller to be combined with this thermal controller. (see Hale and Hardt, 1990), to be combined with this thermal controller.

The ability of the infrared camera to perform rapid line-scan radiation measurements (0.6s /line) also motivates the redefinition of the remaining two welding outputs (Fig. 8). For the heat affected zone (HZ), instead of specifying the isotherm temperature T_h and controlling its width to w_h, it is possible to specify a sideline parallel to the travel direction at the distance $w_p = w_h$ from the center-line. The control system then regulates the peak temperature on that sideline to $T_p = T_h$. This peak temperature T_p requires a single sensor line-scan along the sideline per sampling period, and is more linear than Hz as a welding output because of the smaller spatial variation of its location (x_p, w_p).

The cooling rate CR, which because of the time differen-

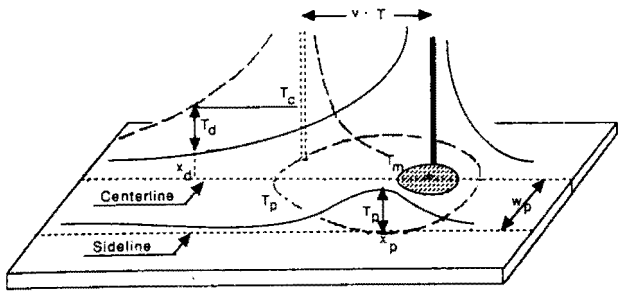

Fig. 8 Definition of the welding outputs T_p and T_d

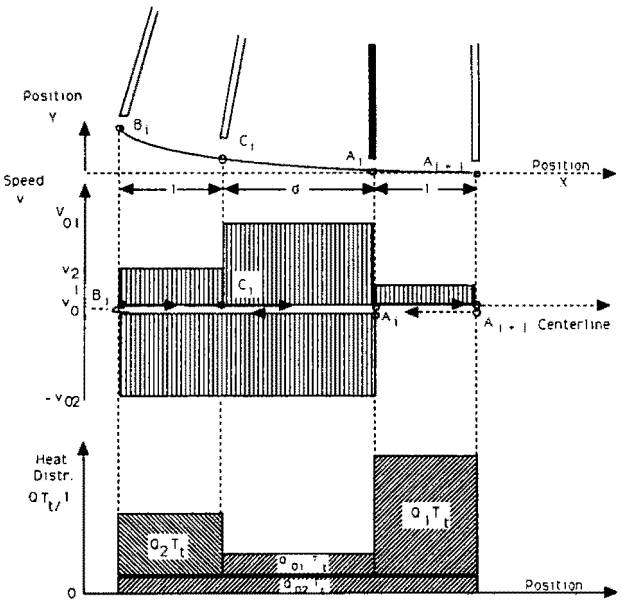

Fig. 9 Torch position, speed, and heat input during a torch cycle

tiation involved requires at least two successive line-scans along the centerline per sampling period, can be integrated over the time T and yield the temperature drop T_d of the centerline point x_d, that was at the critical temperature T_c during the last sampling period (essentially proportional to a backward difference estimate of dT/dt). The evaluation of the temperature drop T_d requires a single sensor line scan along the centerline per sampling period, and it is less noisy than CR as a welding output.

—In selecting the necessary two welding inputs, the torch velocity v was eliminated because of its slowest and most nonlinear influence to the welding outputs (see Table 1, and also Hardt et al., 1985). For the primary and secondary heat inputs Q_1 and Q_2, the implementation problems of a distinct double torch configuration are avoided by time-sharing the same single torch. This is accomplished by performing a cycling motion along the centerline with constant period T_t, which imitates the action of two separate torches at fixed distance $x = d + 1/2$, moving at a constant net common speed $v = 1/T_t$, as in Fig. 9. This figure illustrates the geometry, kinematics and power distribution of the ith torch cycle steps:

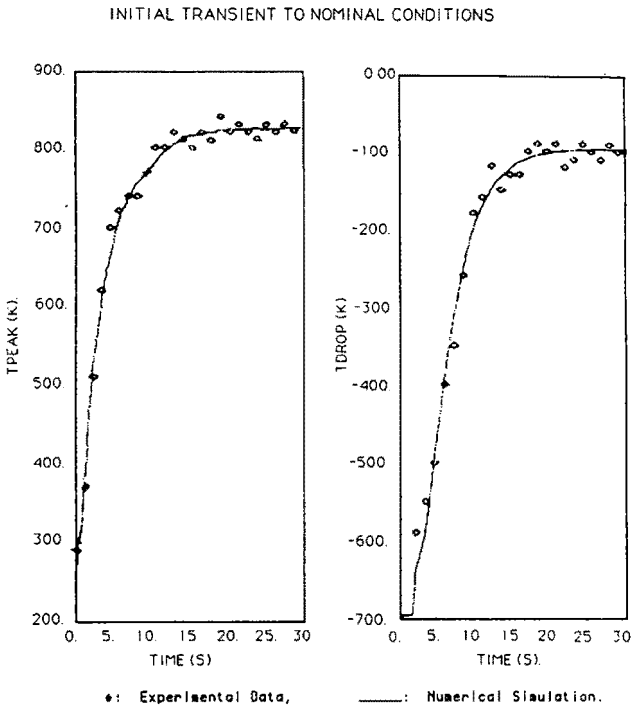

Fig. 10 Time responses of the welding outputs T_p and T_d during the transient to the ominal conditions ($Q_1^* = 2500$ W, $Q_2^* = 250$ W)

This step sequence of the torch cycle minimizes the transient effects of the torch variables, i.e., the sectional velocities v_1 and v_2 (selected so that T_t is constant) and arc power Q (held constant during each cycle), which are used for the modulation of the welding inputs Q_1 and Q_2 of the resulting continuous heat distribution along the centerline, as follows:

$$v_1 = (1 + Q_2/Q_1)\ 1/T_t,$$

$$v_2 = (1 + Q_1/Q_2)\ 1/T_t,$$

$$Q = (Q_1 + Q_2)\ T_t/(T_t - t_{01} - t_{02}).$$

Experimental Process Modeling

After defining the welding outputs (T_p, T_d) and inputs (Q_1, Q_2) of the 2×2 configuration, their dynamic dependency is modeled using the same methodology and experimental arrangement as for the 3×3 model.

The experiments involve GMA butt welding of thin mild steel plates performed by a welding robot (Automatix, 1983). The robot implements the torch cycle above with $l = 6$mm, $d = 9$mm, $T_t = 1.2$ s, $x = 12$ mm and $v = 5$mm/s, using fast joint interpolated motion of a single robot joint for the first three segments (exaggerated in Fig. 9). The arc power Q is manipulated through the welding voltage V, so that its product with current I (estimated from the V-I characteristics of the power supply) provides the necessary $Q = VI$. The IR imaging camera (Inframetrics Model 600) is used to record thermal data, which is then analyzed off-line by a thermal image processor (Thermoteknix, 1986) to determine T_d, defined for an assumed sam-

Step	Torch Action	Segment	Length	Time	Average Speed	Average Power
1.	Backward Transition	A_iB_i	$-d-l$	$-t_{02}$	$-v_{02}$(full speed)	Q_{02}(residual)
2.	Implementation of Q_2	B_iC_i	$-l$	$-t_2$	$-v_2^i$(variable)	$Q_2^i = Q^i l/v_2^i T_t$
3.	Forward Transition	C_iA_i	$-d$	$-t_{01}$	$-v_{01}$(full speed)	Q_{01} (residual)
4.	Implementation of Q_1	A_iA_{i+1}	$-l$	$-t_{01}$	$-v_1^i$(variable)	$Q_1^i = Q^i l/v_1^i T_t$
Net Cycle Motion		A_iA_{i+1}	$-l$	$-T_t$	$-v$(average)	Q^i(variable)

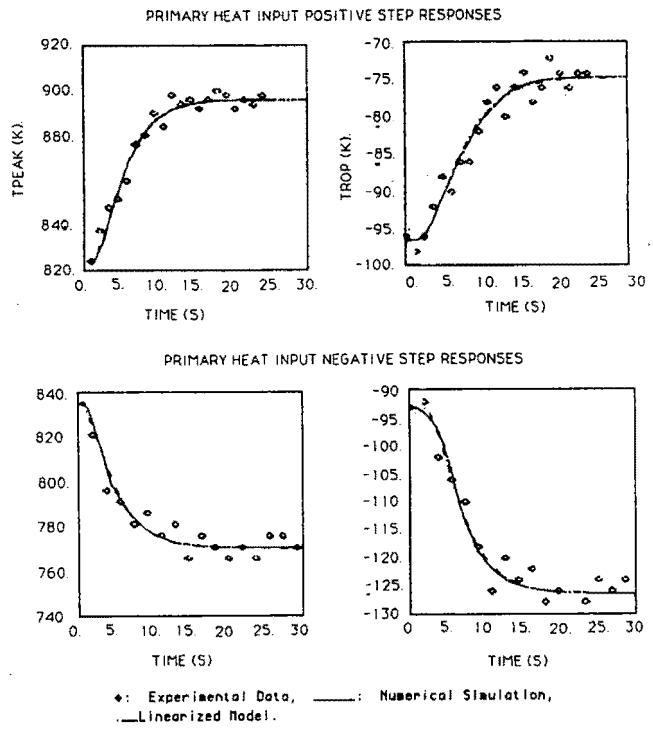

Fig. 11 Time responses of the welding outputs T_p and T_d during a positive and a negative step to Q_1 (from $Q_1{}^* = 2500$ W to $1.2Q_1{}^* = 3000$ W or $0.8Q_1 = 2000$ W)

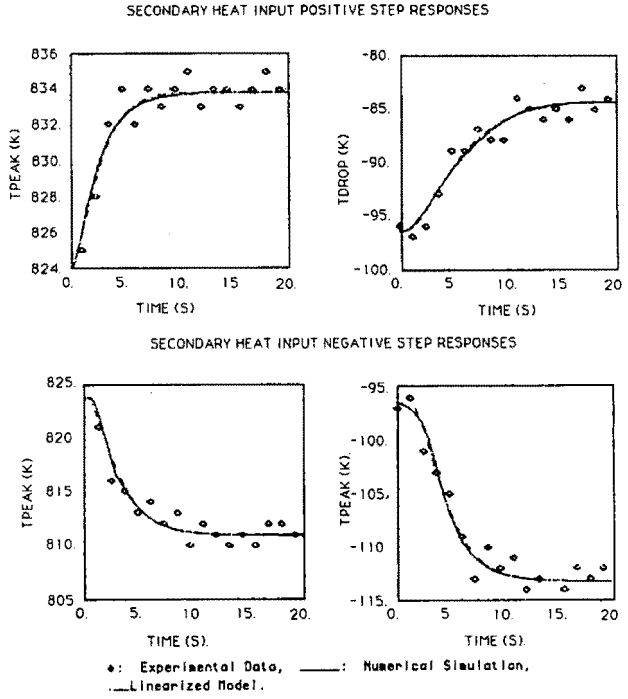

Fig. 12 Time responses of the welding outputs T_p and T_d during a positive and a negative step to Q_2 (from $Q_2{}^* = 250$ W to $2Q_2{}^* = 500$ W or to $QQ_2{}^* = 0.0$W)

Table 2 Transfer function parameters of the linearized model α

Output / Input		Tpeak at Wp=10.5 mm Tp (K)				Tdrop at T=2.4 s Td (K)			
I	Step	K (K/W)	d (s)	w (rad/s)	T_{eq} (s)	K (K/W)	d (s)	w (rad/s)	T_{eq} (s)
Q_1 (W)	$+2Q_1^*$	0.144	1.0	0.410	4.38	0.0441	1.4	0.313	6.39
	$-2Q_1^*$	0.150	1.2	0.352	5.68	0.0546	1.7	0.321	6.24
	$+Q_2^*$	0.0394	0.	0.665	3.01	0.0489	0.2	0.357	5.60
	$-Q_2^*$	0.0522	0.	0.625	3.20	0.0671	0.6	0.476	4.20

(α: standard)

pling period $T = 2.4$s, using the centerline profile, and also to determine T_p, from the thermal profile at distance $w_p = 10.5$ mm.

Thus, the parameters of the numerical simulation (arc efficiency, heat distribution, equivalent conduction in the weld pool) are calibrated so that its responses fit the experimental data during the transition to the new nominal conditions (Fig. 10):

$$Q_1{}^* = 2500 \text{ W corresponding to: } T_p{}^* = 824 \text{ K}$$

$$Q_2{}^* = 250 \text{ W} \qquad T_d{}^* = -96.5 \text{ K}$$

Since T_d is not defined during the first $T = 2.4$s, an upper bound of $|T_d| = T_c - T_o$ is used instead, where T_o is the preheat temperature.

Starting at these nominal conditions, the process dynamics are identified by obtaining the responses of the welding outputs T_p and T_d to both positive and negative steps of each welding input Q_1 and Q_2 separately, both by experiment (diamonds) and numerical simulation (solid line) in Figs. 11 and 12:

(*a*). Positive step of Q_1, from $Q_1{}^*$ to 1.2 $Q_1{}^*$ (Fig. 11(*a*))
(*b*). Negative step of Q_1, from $Q_1{}^*$ to 0.8 $Q_1{}^*$ (Fig. 11(*b*))
(*c*). Positive step of Q_2, from $Q_2{}^*$ to 2.0 $Q_2{}^*$ (Fig. 12(*a*))
(*d*). Negative step of Q_2, from $Q_2{}^*$ to 0.0 $Q_2{}^*$ (Fig. 12(*b*))

These transient responses can be approximated by a delayed, critically damped, second order behavior (see dot-dashed line), corresponding to a secant linearization of the nonlinear process model in the neighborhood of the nominal conditions, described by the transfer functions:

$$\begin{aligned}
\frac{T_p}{Q_1}(s) &= \frac{K_1 e^{-d1s}\omega_1{}^2}{(s+\omega_1)^2} \cong \frac{K_1 e^{-d1s}}{\tau_{eq1}s+1} \\
\frac{T_p}{Q_2}(s) &= \frac{K_2 e^{-d2s}\omega_2{}^2}{(s+\omega_2)^2} \cong \frac{K_2 e^{-d2s}}{\tau_{eq2}s+1} \\
\frac{T_d}{Q_1}(s) &= \frac{K_3 e^{-d3s}\omega_3{}^2}{(s+\omega_3)^2} \cong \frac{K_3 e^{-d3s}}{\tau_{eq3}s+1} \\
\frac{T_d}{Q_2}(s) &= \frac{K_4 e^{-d4s}\omega_4{}^2}{(s+\omega_4)^2} \cong \frac{K_4 e^{-d4s}}{\tau_{eq4}s+1}
\end{aligned} \tag{9}$$

The first-order approximations will be used in the next section to simplify the controller parametrization.

The transfer function parameters, identified by fitting the responses of the linearized model to the previous experimental data, are collected in Table 2, and attest to the expected improvement of the linearity of the 2×2 model, indicated by the narrower variation ranges relative to those of the 3×3 model (Table 1). However, the dynamics are now slower and more coupled, because of the continuous heat distribution and the new nominal conditions with increased total arc power, and thus T_h, T_c isotherm size. With more distant measurement locations of the welding outputs more time is required for the heat diffusion.

These last effects can be countered by a modification of the welding outputs T_p and T_d. By using a sideline at shorter distance $w_p' = 6.8$mm from the centerline (e.g., corresponding to the austenitization rather than recrystallization zone of the material Doumanidis, 1988), and a shorter sampling period $T' = 1$ s, modified outputs T_p' and T_d' are defined. The corresponding parameters of similar transfer functions, derived by linearization of the numerical simulation responses

Table 3 Transfer function parameters of the linearized model β

Input		Output: Tpeak at Wp=10.5 mm Tp (K)				Tdrop at T=2.4 s Td (K)			
I	Step	K (K/W)	d (s)	w (rad/s)	T_{eq} (s)	K (K/W)	d (s)	w (rad/s)	T_{eq} (s)
Q_1 (W)	$+2Q_1^*$	0.239	0.50	0.778	2.57	0.0340	0.96	0.439	4.55
	$-2Q_1^*$	0.250	0.55	0.735	2.72	0.0439	1.06	0.493	4.05
	$+Q_2^*$	0.0008	0.	-	0.	0.0405	0.14	0.533	3.75
	$-Q_2^*$	0.0028	0.	-	0.	0.0421	0.34	0.794	2.52

(β: standard)

to the same series of step inputs in the neighborhood of the nominal conditions:

$$Q_1^* = 2500 \text{ W} \text{ corresponding to: } T'_p{}^* = 996 \text{ K}$$

$$Q_2^* = 250 \text{ W} \qquad T'_d{}^* = -56.4 \text{ K}$$

are systematized in Table 3. These indicate the decoupledness of T_p' from Q_2 and the faster dynamics of the modified 2×2 model, since the measurement locations of the welding outputs T_p' and T_d' are closer to the heat source.

Implementation of the Control System

Following the methodology of the design section, the multivariable, adaptive, deadbeat controller with input saturation, adaptation gain adjustment and the external secondary loop (Fig. 2), is redesigned on the basis of the 2×2 process model, with its experimental implementation requirements in mind. The parametrization of this *standard* 2×2 controller, as well as the initial parameter estimates $-i$, are obtained by discretization of the linearized reduced model above, with $\mathbf{u}(t) = Q_1\ Q_2]^T$, $\mathbf{y}(t) = [T_p\ T_d]^T$, i.e., $r=m=2$. The sampling period was chosen as $T=T_t = 2.4$ s, corresponding to the smallest integer number of torch cycles (for synchronous operation) that also satisfies the algorithm assumptions (such as all process delays being less than 2.4 seconds) and that could be implemented.

The *simplified* 2×2 controller design was based on the delayed first order approximate model, since its parametrization (sampled polynomial orders $n_1=n_2=m_1=m_2 = 2$, requiring 12 Θ_i components) was found to yield better closed-loop bandwith than with the controller based on the delayed second order model (polynomial orders $n_1=n_2=m_1=m_2=4$, requiring 28 Θ_i components).

Finally, to attempt an improvement in the response time of the control system, a similar *modified* 2×2 controller was designed for the modified 2×2 model of the last section (where the outputs were $\mathbf{y}'(t) = [T_p'\ T_d']$). This model permits a sampling period of $T' = 1$s and has only 8 Θ_i' components, because of its faster dynamics and decoupledness (Table 3).

The experimental implementation of the closed-loop thermal control system is illustrated in Figs. 13 and 14. The thermal camera is arranged to the weld line obliquely from the side, and the field of view is such that the entire length of the weld (300 mm) is within the field of view. (See Doumanidis 1988 for details). The *simplified* 2×2 12-parameter algorithm developed above is implemented in Turbo Pascal executed by an AT&T PC 6300 microcomputer. The initial parameter estimates $\Theta_i(0)$ are based on an *a priori* external calibration.

During the tests of the next section, the closed-loop operation starts after the nominal conditions are reached. Then the system is either issued a new reference command or encounters a process disturbance. Each sampling period begins when a synchronization signal is transmitted from the robot to the controller, at which time the welding robot starts the first torch cycle. After waiting to compensate for the process delays, the computer sets the IR camera to the measurement mode by

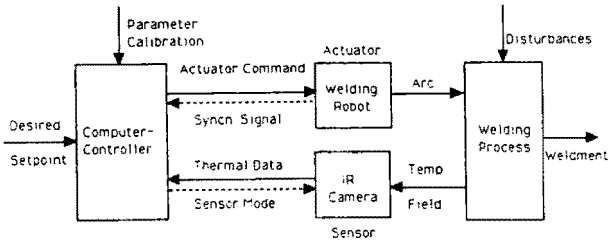

Fig. 13 Control equipent communication diagram

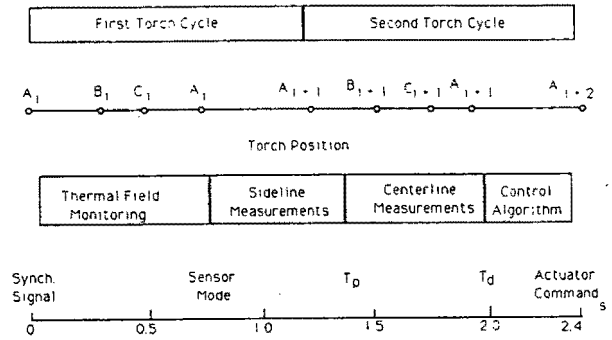

Fig. 14 Actuator and controller synchronization diagram

sensor modal commands transmitted via a serial communication line. The infrared camera senses the welding temperature field and transmits back to the computer (via the same line) the radiation values first of the sideline and then of the centerline locations. Because of the longer delays associated with the temperature drop T_d on the centerline than with the peak temperature T_p on the sideline (Table 2), this procedure ensures better conditioning of the matrix of leading parameters $[b_{ij}^o]$. The camera is then reset to the monitoring mode for the remaining portion of the sampling period to record recording thermal images for off-line processing. This is why the experimental data obtained during the tests of the next section cannot be continuous in time.

Next, the welding outputs T_p and T_d are evaluated in-process from the measured radiation values, on the basis of the Stefan-Boltzmann law and the control algorithm determines the necessary welding inputs Q_1 and Q_2 for their regulation to T_p^d, T_d^d. Thus, the actuator variables, i.e., the sectional velocities v_1 and v_2 and the welding voltage V, can be computed from Q_1, Q_2 according to the previous formulae and the experimental I(V) relationship for the power supply torch combination, and can be transmitted as a command to the welding robot through a second serial communication line. Lastly, the computer saves the current sampling period results and waits for a new synthronization signal, at which time the robot has completes the second torch cycle and adjusts to the new values of the actuator variables for the next sampling period. This routine is repeated until the full test weld bead length is deposited.

Performance of the Thermal System

The performance of the closed-loop system with the *standard* 2×2 controller is tested both by simulation and experiment, with equivalent continuous heat distribution and controller delays. First, the welding output and input responses of the experimental servosystem during tracking a substantial step reference command at $t=0$ to a different operating point:

$$T_p^d = 883 \text{ K} \text{ corresponding to: } Q_1 = 2750 \text{ W}$$

$$T_d^d = -72.5 \text{ K} \qquad Q_2 = 500 \text{ W}$$

are shown in Fig. 15, together with the respective computational transients of the linearized model (dot-dashed) and numerical

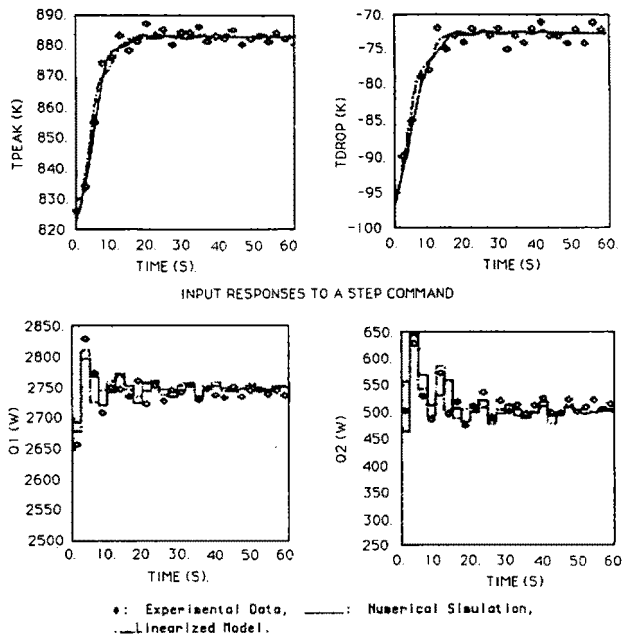

Fig. 15 Time responses of the welding outputs and inputs after a step reference command (*simplified* 2×2 system)

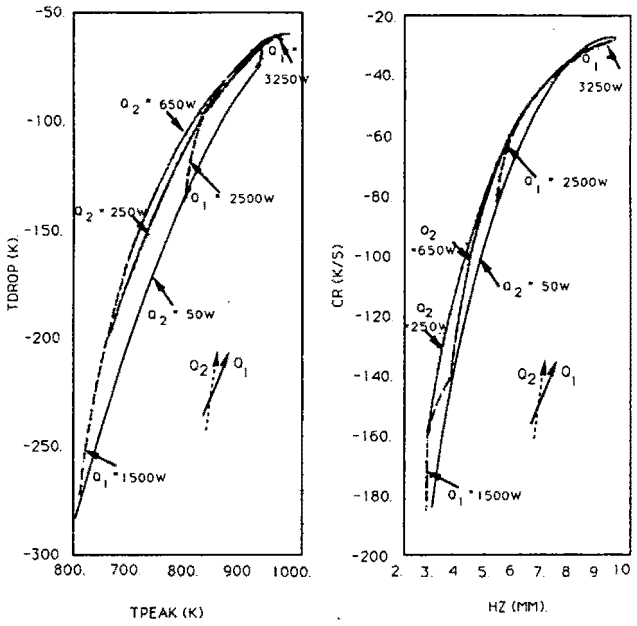

Fig. 16 Achieveable steady-state setpoints of the welding outputs (T_p, T_d) and (*HZ, CR*)

simulation (solid line). As before, the differences between these responses are because of modeling imperfections. The desired welding outputs are tracked exactly at the steady state, and the transients are smooth because of the mild input modulation, although the setting length is about 70 mm. Notice that the HAZ size can be served more directly by displacing in real-time the sideline, i.e., the location of the camera scan line, from w_p relative to the centerline to the desired weld zone (T_h isotherm) width w_p^d, still keeping $T_p^d = T_p^* = T_h$. However, because of the different process dynamics at the new sideline position, the control law is faced with Θ_i parameter changes, resulting in nonsmooth transients and longer setting times.

The approximate ranges of achieveable welding output setpoints of the thermal controller are studied by numerical simulation calibrated at the nominal conditions, and are depicted in Fig. 16 as a mapping of the subspace of unsaturated welding inputs, **u**, to the space of steady-state welding outputs $\mathbf{y}(\,) = [T_p\ T_d]$ (Fig. 16(a)), or $Y(\infty)$ = [HZ CR] (16*b*). The feasible reference setpoints are inside the enveloping line, and clearly there is more control authority in the lower heat input region. Although the I/0 dependencies are coupled, the angles between the two curve families indicate the preferential effect of Q_1 on T_p or HZ, and of Q_2 and T_d or CR, as expected from the gain values and variations in Tables 1 and 2. At the high total arc power region, there is little further flattening of the local temperature hill slope at the critical centerline point x_d, as it shifts backwards, and thus little change of T_d or CR, while at the low arc power end the two peaks of the temperature hill are widely separated, and HZ is eventually decoupled from Q_2. The greater nonlinearity of (∞) compared to (∞) is responsible for the more restricted control range in Fig. 16(*b*), as well as for the inverse bifurcation effects at the low power end, which might cause singularities of the control law without the adaptation gain adjustment.

The disturbance rejection behavior of the closed-loop system is tested again using the standard step plate thickness reduction from 3.17 to 2 mm at $t = 0$, (a serious geometrical disturbance), characterized as an additive disturbance $\mathbf{d}(t)$ to the linearized model output (on the basis open-loop numerical simulation) as:

$$T_p\text{: } d_p(t) = 92.8\ (1 - e^{-t/4.5})\ \text{(K)}$$

$$T_d\text{: } d_d(t) = 27.8\ (1 - e^{-t/6.6})\ \text{(K)}.$$

The experimental welding output and input responses are illustrated in Fig. 17, together with the computation ones, with the linearized model (dot-dashed) and the numerical simulation (solid line) as the process model. The disturbance is eventually rejected at the steady state, with limited output deviations during the transient, but with a settling length of about 120mm.

The regulator performance is also tested experimentally for four more step disturbances encountered at $t = 0$ (Fig. 18). A disturbance in the material properties, mainly the thermal diffusivity α and emissivity ϵ, occurs when the torch crosses the boundary between two plates of similar geometry but different material (solid line, crosses). The disturbance in boundary conditions consisted of soaking part of the plate bottom surface in water, thus increasing the heat losses to the environment when the torch enters this part. However, the system responses do not deviate significantly from the nominal conditions and are not plotted in Fig. 18. A temperature field (initial condition) disturbance is implemented by driving the torch into another insulated plates that is preheated by previous welding (dot-dashed line, squares). Lastly, a disturbance in the process conditions is obtained by a step decrease of the average torch velocity to $v = 4$ mm/s, by altering the torch cycle segment lengths $1 = 4.8$ mm, $d = 9.6$ mm, still with $T_t = 1.2$ s (dashed line, x's). In all cases the disturbances are eventually rejected, although with a small steady-state deviation in the case of the material disturbance, since the undetectable change in surface emissivity deceives the temperature measurements by the infrared radiation pyrometer. There are initial temperature field distortion effects at the boundary of separate plates (in the material and preheat case), and the steady-state input values after the velocity and preheat disturbance, given the stronger effect of Q_2 on T_d, indicate the preferential effect of preheat on the cooling rate.

The performance of the *modified* 2×2 closed-loop system (where the redefined welding outputs T_p' and T_d' is used) are assessed by simulation only since the required sampling time of 1s could not be implemented owing to speed limitation for

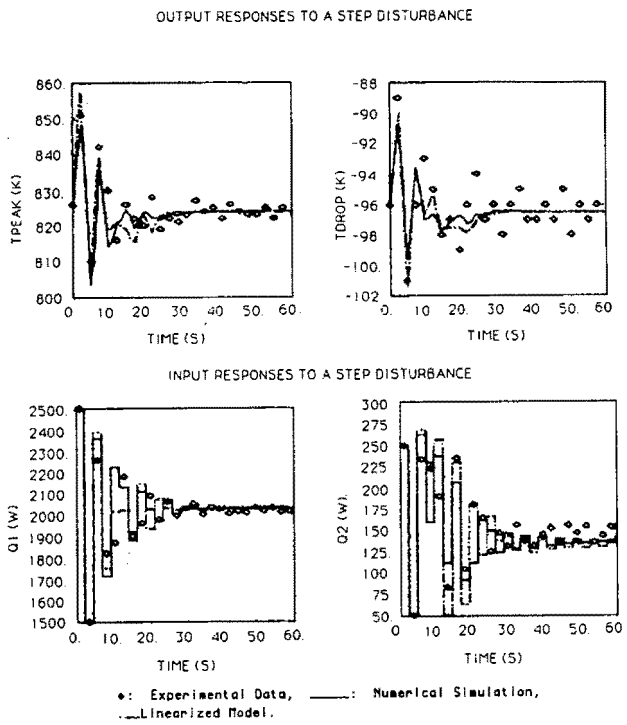

Fig. 17 Time responses of the welding outputs and inputs after a step thickness disturbance (*simplified* 2×2 system)

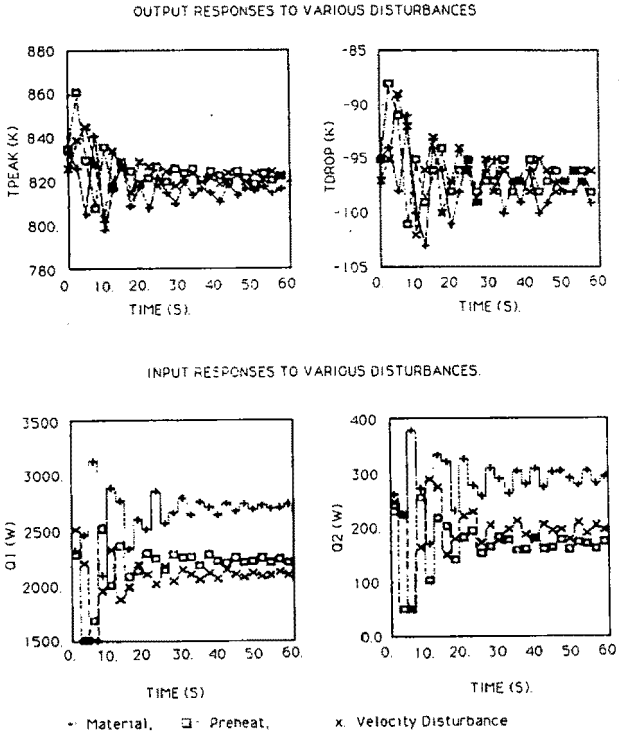

Fig. 18 Time responses of the welding outputs and inputs after various step disturbances (*simplified* 2×2 system)

the sensor and actuator. the command following responses of the welding outputs and inputs after a step reference command from the nominal conditions ($T_p'^*, T_d'^*$), to the new operating point:

$$T'^{\,d}_p = 1056 \text{ K} \quad \text{corresponding to:} \quad Q_1 = 2750 \text{ W}$$

$$T'^{\,d}_p = -40.4\text{K} \qquad\qquad Q_2 = 500 \text{ W}$$

are shown in Fig. 19, for both the linearized model (dot-dashed) and the numerical simulation (solid line). The disturbance rejection behavior is tested using the standard step thickness reduction disturbance $\mathbf{d}(t)$, with the closed-loop responses shown in Fig. 20. In both the input step and disturbance rejection tests, the attractive time domain performance stems from the speed and decoupledness of the modified 2×2 process model, enabling the use of a similer parametrization and shorter sampling period by the *modified* 2×2 controller.

Conclusion: Limitations and Applicability

This paper presents a method for modeling and controlling two key thermal characteristics of welding in real-time. The basic system is a distributed parameters, non-linear process, and a lumped parameter locally linear model is used to design a dead-beat adaptive control system. The general performance of such a system is assessed both through simulation (using a full finite difference implementation of the process model) and through full scale experiments. The response characteristics of the closed-loop thermal control system generally satisfy the design specifications, and the benefits of the adaptive strategy are apparent (indeed, several of the disturbances presented cannot be handled by fixed parameter controllers, see Doumanidis, 1988).

However, there are still performance limitations, primarily bandwidth, arising both from equipment and methodology limitations. Among the welding process characteristics, the importance of speed and decoupledness of its dynamics is demonstrated by comparison of the performances of the *standard and modified* 2×2 control systems. Definition of the welding outputs close to the heat source is essential for process

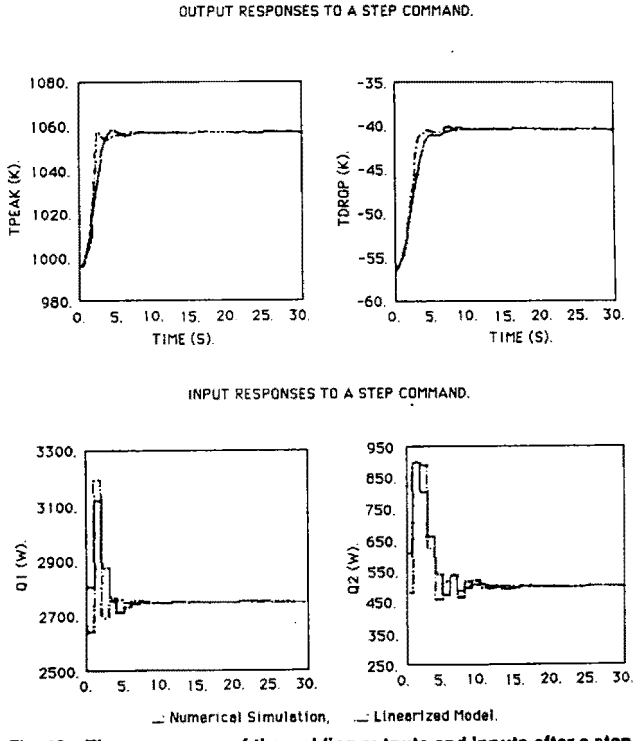

Fig. 19 Time responses of the welding outputs and inputs after a step reference command (*modified* 2×2 system)

model speed, while decoupledness is additionally favored by small thermal diffusivity a and long equivalent torch distance x. The welding input modulation range, limited by input saturation to avoid catastrophic melt-through or extensive porosity and lack of fusion, should be maximized by proper experimental selection of the nominal conditions. This is also essential to avoid the GMAW process noise, stemming from arc instabilities and the globular metal transfer mode.

The bandwidth limitations are primarily imposed by the slow measurement speed of the thermal sensor. The time-consuming, sequential radiation measurements first on the sideline and then on the centerline provide time-shifted welding output estimates T_p and T_d, thus introducing unequal controller delays and deteriorating its conditioning. The resulting Nyquist frequency of sampling $\omega_N = \pi/T = 11.31$ rad/s poses and upper limit to the welding output frequency components that can be sensed without aliasing, although the dominant process frequencies of Tables 2 and 3 are well below it. The temperature resolution of the infrared pyrometer (1K) and the resulting quantization may inhibit fine regulation of the welding outputs. The spatial camera resolution (1.2 mm longitudinal X 0.2 mm transverse) poses an upper bound to the monitored length of weld bead. The sphericity of the camera field of view, i.e., the imagining of straight lines as slightly curved arcs, causes minor misalignment deviations from the line scan axis. Finally, the effects of in-process emissivity variations, as already realized, are inevitable as long as radiation measurements are performed at a single wavelength range, necessitating Emittance Independent Infrared Analysis (EIIA) techniques (Chin et al., 1983). Most of these problems can be avoided by adopting a multiplexed, discrete-point, fiber optic array sensor (Boillot et al. 1985), with its focusing system and fiber head attached to the welding torch, to measure temperatures at a limited number of sideline and centerline locations, which also avoids the bulkiness, fragility, cost and electromagnetic interference from the arc of the infrared camera system.

The dynamics of the process actuator, i.e., the mechanical manipulator and power supply, are also subject to speed limitations affecting the system performance. Since the torch cycling frequency $\omega_t = 2\pi/T_t = 5.236$ rad/s is about one order of magnitude higher than the dominant process frequencies (Table 2), the resulting dynamic components of the welding inputs are attenuated about 100 times by the quasi-second order process dynamics, so that the welding outputs are affected only by the static, averaged input components. However, with the faster dynamics of the modified system (Table 3), there is less low-pass filtering of the cycling frequency input components, which may affect the welding outputs. Apart from proper step sequence and synchronization of the torch cycle to controller sampling, a faster torch cycling system may be implemented, either as a dedicated mechanism or arc magnetic deflection device (Essers and Walter, 1981), attached as the end effector of the welding robot. Also, bead contour variations caused by the rapid torch motion may as well required the use of a separate secondary torch trailing the first. This would be an autogenous gas tungsten arc torch.

The importance of the sampling period and model parametrization on controller adaptation performance, together with the restrictions of input saturation, have been demonstrated. Since inaccuracies of the initial off-line controller parameter estimates $\Theta_i(0)$ degrade the initial transient performance of the thermal system, their initialization should be obtained by a self-calibration closed-loop operation period at the nominal conditions before service. Additional computational requirements can be handled, and the controller delay can be shortened, by dedicated hardware executing optimized code. Finally, weld bead geometry controllers (outlined in Hale and Hardt, 1990) or even residual stress and distortion regulators can be combined to this microstructure and material properties control system, providing integrated welding process control.

In its current experimental configuration, the thermal control system is most applicable to straight or slightly curved, medium length (limited by the settling length and longitudinal camera resolution) seams of arbitrary cross section, as long as the centerline and sideline are accessible by the sensor. The limited closed-loop band-width is suitable to materials of low and medium thermal diffusivity (e.g., steels), while high- materials (e.g., aluminum) require faster experimental equipment to take advantage of their rapid dynamics (see Doumanidis (1988) for numerous material case studies). Clean, smooth and uniform plate surfaces, without emissivity variations (fluxes, stain, paint etc.) or orientation fluctuations (ripples, spatter, asperities etc.) are always preferable. Finally, the application range if thermal control system covers most welding application range of the thermal control system covers most welding techniques (GTAW, GMAW etc.) in industrial practice, including pressure vessel fabrication, shipbuilding, various constructions etc.

References

Astrom, K. J., and Wittenmark, B., *Computer Controlled Systems, Theory and Design*, 1984, Prentice-Hall.

Automatrix, Inc., 1983, "Rail Software Reference Manual for Robovision and Cybervision Systems," MN-RB-07, Billerica MA, Oct.

Boillot, J. P., Cielo, P., Begin, G., Michel, C., Lessard, M., Fafard, P., and Villemure, D., 1985, "Adaptive Welding by Fiber Optic Thermographic Sensing: An Analysis of Thermal and Instrumental Considerations," *Welding Journal*, July, pp. 209s-217s.

Chin, B. A., Madsen, N. H., and Goodling, J. S., 1983, "Infrared Thermography for Sensing the Arc Welding Processes," *Welding Journal*, Sept. pp. 227s-234s.

Doumanidis, C. C., 1988, "Modeling and Control of Thermal Phenomena in Welding," Ph.D. thesis, Department of Mechanical Engineering, MIT, Jan.

Doumanidis, C. C., Hale, M., and Hardt, D.E., 1986, "Multivariable Control of Arc Welding Processes," *Trends in Welding Research, ASM*, May, pp. 449-460.

Doumanidis, C. C., and Hardt, D. E., 1988, "Modeling of Thermal Properties in Welding," to be published in ASME JOURNAL OF DYNAMIC SYSTEMS, MEASUREMENT AND CONTROL, Vol. 110.

Doumanidis, C. C., Hale, M. B., and Hardt, D. E., 1987, "Non-Linear Dynamics on Welding Control Modelling," *Proc. Symposium on Problems in Energy Engineering*, June.

Essers, W. G., and Walter, R., 1981, "Heat Transfer and Penetration Mechanisms with GMA and Plasma GMA Welding," *Welding Journal*, Vol. 60, 1981, p. 37s-42.

Goodwin, G. C., Ramadge, P. J., and Caines, P. E., 1980, "Discrete-Time Multivariable Adapative Control," *IEEE Trans. on Automatic Control*, Vol. AC-25, No. 3, June, pp. 449-456.

Hale, M. B., and Hardt, D. E., 1990, "Multivariable Geometry Control of Gas-Metal Arc Welding: Controller Design," *Proc. ASME Symposium Modeling and Control of Manufacturing Processes*, Dallas, Nov.

Hale, M., 1989, "Multivariable Control of a GMA Welding Process," Ph.D. thesis, MIT, Sept.

Hardt, D. E., Garlow, D. A., and Weinert, J. B., 1985, "A Model of Full Penetration Arc-Welding for Control System Design," ASME JOURNAL OF DYNAMIC SYSTEMS, MEASUREMENT AND CONTROL, Vol 107, Mar.

Inframetrics Inc., "Installation and Operation of the Inframetrics Model 600 IR Imagining Radiometer," 4625 Rev. B., Bedford, MA, Dec. 1985.

Nomura, H., et al., 1980, "Arc Light Intensity Control Current in SA Welding System," *Journal of Welding and Metal Fabrication*, Sept.

Rohrs, C. E., and Sirriani, J. M., 1986, "Robust Adaptive Control in Sampled Data Systems," Lecture given at MIT, Oct.

Rosenthal, D., 1941, "Mathematical Theory of Heat Distribution During Welding and Cutting," *Weld J.*, Vol. 20(5), pp. 220s-234s.

Suzuki, A., and Hardt, D. E., 1987, "Application of Adaptive Control to Weld Geometry Control," *Proc. ACC*, June.

Thermoteknix Systems Ltd., 1986, "Operating Instructions for the Thermagram Thermal Image Processing System," Cambridge UK, Jan.

Valavani, L., 1986, "Adaptive Control," Lecture Notes for 16.375, Department of Aeronautics and Astronautics, MIT, Fall.